Doping effects in high-harmonic generation from correlated systems

Thomas Hansen◉ and Lars Bojer Madsen◉

Department of Physics and Astronomy, Aarhus University, DK-8000 Aarhus C, Denmark

Using the one-dimensional Hubbard model, which is commonly used for describing, e.g., high-T_c superconducting cuprates, we study high-harmonic generation (HHG) from doped, correlated materials. Doping is modeled by changing the number of electrons in the lattice from the conventional half-filling case. For relatively small Hubbard U, i.e., small electron-electron correlation, we find little to no effect of doping on the dynamics and the HHG spectra. For increasing U the degree of doping has a marked effect on the dynamics and spectra. We explain these findings through the quasiparticle-based doublon-holon picture. The dynamics are separated into two types, first, doublon and holon movement, and, second, doublon-holon pair creation and annihilation. Doping results in all configurations containing doublons or holons. Those quasiparticles can move at no extra cost in energy regardless of the correlation level. This motion at no energy cost increases the high-harmonic gain for low- and medium-harmonic orders. We discuss that in the high-U limit, antiferromagnetic ordering becomes increasingly unlikely with increasing doping rates and explain an associated drop in the high-order harmonics relative to the case of half-filling.

I. INTRODUCTION

High-harmonic generation (HHG) is a highly nonlinear, ultrafast, attosecond to femtosecond (10^{-18}–10^{-15} s) process through which ultrashort laser pulses, with high photon energy can be produced [1–5]. The HHG process also allows for retrieval of spectrographic information of the generating materials at a subfemtosecond timescale [4,6–10]. A prominent description of the HHG process in solids originates from the Bloch-band picture and splits the dynamics into two types: intraband and interband HHG [11,12]. The intraband HHG arises from a charge carrier propagating through a curved Bloch band, the underlying acceleration results in radiation. The interband HHG is best described using the so-called three-step model: (i) an electron is excited across a band gap, (ii) the excited electron and created hole propagate through their respective bands, resulting in intraband radiation, and (iii) the hole and electron recombine thus emitting a photon with energy given by the energy difference between the conduction and valence bands in question at the crystal momentum at the time of recombination [12].

Since the first observation of HHG from solids [5], it has garnered much interest, as the higher particle density as compared to gases could enable the production of higher intensity ultrafast pulses [1,9,13–22]. Recently, research into HHG from highly correlated materials, such as Mott insulators, has received much interest both theoretically [10,23–35] and experimentally [36–38]. The Hubbard model has been used in this context as it captures certain aspects of the physics in real materials [39,40]. One such class of materials is cuprates. Cuprates contain high-temperature superconductors and therefore much research towards understanding the mechanism leading to superconductivity in cuprates and

pushing their critical temperature higher has been done [41,42]. As a result, it is highly interesting to elucidate the transport properties of such materials, e.g., through HHG. In all cuprate materials, the onsite electron repulsion plays a significant role in the dynamics of the system. They can therefore be described as, potentially, doped Mott insulators [39,40]. Note that the metal-insulator transition generally happens for solids with only full, empty, or half-filled bands, i.e., Mott insulators are only achieved when every band is either full, empty, or half-filled. Another group of materials, some of which can be simulated by similar Hubbard-model-based techniques, are the nearly one-dimensional organic charge-transfer salts. These salts can range from Mott insulators, through organic metals, to superconductors [43].

This leads us back to the predominant model for studying correlated materials, the Hubbard model. Onsite electron-electron repulsion is included through the so-called Hubbard-U term. This model is frequently used to study HHG from Mott insulators [10,23,24,34]. Such studies have led to a three-step model formulated in terms of doublon and holon quasiparticles. Doublons are doubly occupied lattice sites, and holons are empty sites. The three steps are as follows: (i) A doublon-holon pair is created, (ii) the created doublon and holon propagate throughout the lattice, and (iii) the doublon-holon pair recombines under emission of a high-energy photon [24].

Studying HHG from Mott insulators requires the half-filling assumption. However, cuprates include materials for which the highest occupied band is far from half-filled [40]. It is noted that one-dimensional cuprate chains have been synthesized with many different degrees of hole doping [44]. As the degree of band filling is of extreme importance to the dynamics [43] it is of interest to go beyond the assumption of

half-filling and address its influence on the ultrafast dynamics in correlated materials through the nonlinear process of HHG. Especially as half-filling is a special case in correlated materials since the ground state contains neither doublons nor holons for $U \to \infty$. So here we present a study of HHG using the Hubbard model for non-half-filling cases. Our goal is to elucidate the following questions: (i) What effects does doping away from half-filling have on the HHG spectra? (ii) How do the dynamics of non-half-filled bands differ from half-filled bands? (iii) How do the changes in the dynamics and HHG spectra relate to one another?

The paper is organized as follows. In Sec. II, the theoretical model and numerical methods are introduced. In Sec. III, the results are presented and analyzed and, finally, in Sec. IV we conclude. Atomic units are used throughout unless stated otherwise.

II. THEORETICAL MODEL AND METHODS

We work with the one-band Hubbard model on a one-dimensional chain of $L = 12$ atoms with periodic boundary conditions. We use different numbers of electrons, keeping the number of spin-up and -down electrons equal at all times to consider spin-neutral situations for a range of different degrees of band filling.

In the presence of a driving laser pulse, the Hubbard model Hamiltonian can be expressed as [45]

$$\hat{H} = -t_0 \sum_{i,\sigma} (e^{iaA(t)} \hat{c}_{i+1,\sigma}^\dagger \hat{c}_{i,\sigma} + \text{H.c.}) + U \sum_i \hat{n}_{i,\uparrow} \hat{n}_{i,\downarrow}, \quad (1)$$

where t_0 is the nearest-neighbor hopping matrix element which, by lattice symmetry, is independent of lattice site and hopping direction. An electromagnetic field is included via Peierl's phase $e^{\pm iaA(t)}$ where a is the lattice spacing and $A(t)$ is the electromagnetic vector potential treated in the electric dipole approximation, i.e., neglecting the spatial dependence in $A(t)$. The fermionic creation and annihilation operators for an electron on site i with spin $\sigma \in \{\uparrow, \downarrow\}$ are denoted by $\hat{c}_{i,\sigma}^\dagger$ and $\hat{c}_{i,\sigma}$, respectively. The electron-electron correlation is included via the Hubbard-U term. U will be treated as a parameter. Finally, $\hat{n}_{i,\sigma} = \hat{c}_{i,\sigma}^\dagger \hat{c}_{i,\sigma}$ is the number operator for electrons on site i with spin σ. It is seen from the last term in Eq. (1) that each doublon increases the energy in the system by U. The values for lattice spacing and hopping term were picked to fit those of Sr_2CuO_3 [46], as was done previously in Ref. [10]. The specific values are $a = 7.5589$ a.u. and $t_0 = 0.0191$ a.u.

We use a linearly polarized, $N_c = 10$ cycle pulse with polarization direction along the lattice dimension. We use a $\sin^2$ envelope. The explicit form of the vector potential is

$$A(t) = A_0 \cos(\omega_L t - N_c \pi) \sin^2\left(\frac{\omega_L t}{2N_c}\right). \quad (2)$$

The vector potential amplitude is given by $A_0 = F_0/\omega_L = 0.194$ a.u. and the angular frequency by $\omega_L = 0.005$ a.u.$= 33$ THz. The field strength F_0 corresponds to a peak intensity of 3.3×10^{10} W/cm^2.

Nonvanishing values of U lead to a Mott gap. In the $U = 0$ limit, the model reduces to that describing a single Bloch band, i.e., in this limit only intraband dynamics occur.

Note that intraband models have been successful in describing HHG from a variety of materials [5,9,14–17,47].

The simulations are done by solving the time-dependent Schrödinger equation via the Arnoldi-Lancoz algorithm [48–51]. This goes for both the imaginary-time propagation used to find the initial ground state and the real-time propagation. The imaginary-time propagation continues until the energy is converged and the electron density is translationally symmetric. The latter is required by translation symmetry of the lattice. We find that the symmetry requirement is the stricter of the two when starting the imaginary-time propagation from a random initial state. We test that we achieve convergence of the real-time propagation by comparing spectra and currents for increasing Krylov subspace dimension and decreasing time step. In practice this means we use a maximal Krylov subspace dimension of 4 and a time step of 1 a.u. In the case of half-filling and $U = 0.1t_0$ we needed to decrease the time step by a factor of 10 to 0.1 a.u. in order to achieve convergence.

We consider a target that is thin in the laser propagation direction. This allows us to neglect propagation and phase-matching effects [52]. In this case, the generated field is proportional to the electron acceleration, i.e., the time derivative of the current. Therefore the spectrum $S(\omega)$ is expressed as

$$S(\omega) = \left| \mathcal{F}\left(\frac{d}{dt} j(t)\right) \right|^2 = |\omega j(\omega)|^2, \quad (3)$$

where $j(\omega)$ is the Fourier transform ($\mathcal{F}$) of the current $j(t) = \langle \hat{j}(t) \rangle$. Here the current operator reads as [53]

$$\hat{j}(t) = -iat_0 \sum_{i,\sigma} (e^{iaA(t)} \hat{c}_{i+1,\sigma}^\dagger \hat{c}_{i,\sigma} - \text{H.c.}). \quad (4)$$

In the analysis of our results, we will utilize a separation of the current into two parts. These are the currents associated with the movement of doublons and holons and the current associated with the creation or annihilation of doublon-holon pairs. This separation is in line with the earlier mentioned parallel to the three-step model. The creation and annihilation dynamics are parallel to interband dynamics, and the doublon and holon hopping dynamics are parallel to intraband dynamics [23]. As the U term of Eq. (1) effectively counts the number of doublons, this distinction is physically relevant. Following Ref. [24], we denote these currents as $j_{ca}(t) = \langle \hat{j}_{ca}(t) \rangle$ and $j_{hop}(t) = \langle \hat{j}_{hop}(t) \rangle$ respectively. Here "ca" refers to the creation and annihilation of doublon-holon pairs, and "hop" refers to the current associated with the hopping of doublons and holons. The current operator can be expressed as $\hat{j}(t) = \hat{j}_{ca}(t) + \hat{j}_{hop}(t)$ with [24]

$$\hat{j}_{ca}(t) = iat_0 \sum_{i,\sigma} [e^{iaA(t)} (\hat{d}_{i,\sigma}^\dagger \hat{h}_{i+1,\sigma}^\dagger + \hat{h}_{i,\sigma} \hat{d}_{i+1,\sigma}) - \text{H.c.}], \quad (5)$$

$$\hat{j}_{hop}(t) = iat_0 \sum_{i,\sigma} [e^{iaA(t)} (\hat{h}_{i,\sigma} \hat{h}_{i+1,\sigma}^\dagger + \hat{d}_{i,\sigma}^\dagger \hat{d}_{i+1,\sigma}) - \text{H.c.}], \quad (6)$$

where $\hat{d}_{i,\sigma}^\dagger = \hat{c}_{i,\sigma}^\dagger \hat{n}_{i,\gamma}$ and $\hat{h}_{i,\sigma}^\dagger = \hat{c}_{i,\sigma}(\hat{I} - \hat{n}_{i,\gamma})$ are operators which create a doublon or holon, respectively, on site i by creating or annihilating an electron with spin σ. Note that γ denotes the spin, opposite to σ, and $\hat{I}$ denotes the identity
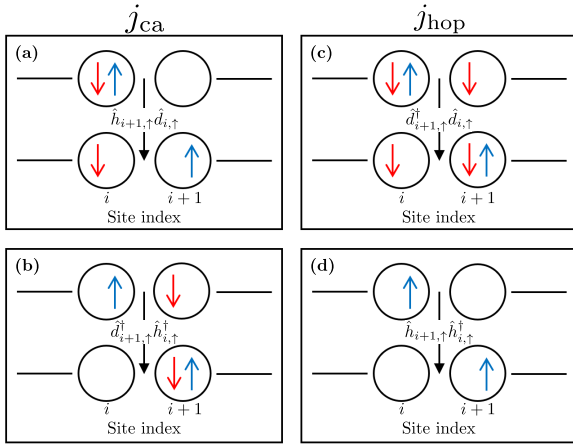
FIG. 1. Illustration of the separation of the dynamics into currents $j_{ca}(t)$ associated with the (a) annihilation and (b) creation of doublon-holon pairs, and into currents $j_{hop}(t)$ associated with the hopping of a (c) doublon or a (d) holon. Sites are illustrated by black circles. In each panel the upper sites are the initial configuration, and the bottom the final configuration. The transition is created by the operator written in the middle of each panel. A red arrow indicates that a spin-down electron occupies the given site, similarly, a blue arrow indicates that a spin-up electron occupies the given site.

operator. The operators achieve their function, in terms of hopping, creation, and annihilation, by effectively doing two things. First, they check whether an electron with spin γ is or is not on the site in question, for doublon or holon manipulation, respectively. Second, they create or annihilate an electron with spin σ on the given site. Figure 1 illustrates examples of the action of terms in Eqs. (5) and (6) describing the hopping of a spin-up electron from site i to site $i + 1$. We see from the figure how these operators (a) annihilate a doublon-holon pair, (b) create a doublon-holon pair, moves (c) a doublon or (d) a holon.

In our analysis of the results, we also consider spectra generated from only $j_{hop}(t)$ and $j_{ca}(t)$, respectively. Those spectra are given by

$$S_{hop}(\omega) = |\omega j_{hop}(\omega)|^2, \quad S_{ca}(\omega) = |\omega j_{ca}(\omega)|^2. \quad (7)$$

Although $S_{ca}(\omega)$ and $S_{hop}(\omega)$ can not be measured individually since $S(\omega) = |\omega j(\omega)|^2 = |\omega j_{ca}(\omega) + \omega j_{hop}(\omega)|^2$, these latter spectra can still indicate the relative importance of each mechanism.

To interpret results regarding this separation of the underlying dynamics, we utilize the measure

$$D(t) = \sum_i \frac{\langle \hat{n}_{i,\uparrow} \hat{n}_{i,\downarrow} \rangle}{L}. \quad (8)$$

This D measure is the expectation value of the U term, of Eq. (1), scaled by $1/(UL)$. The D measure, therefore, provides a way to compare the effects of the U term across different simulations. In the limit of $U \gg t_0$, the eigenstates of Eq. (1) become energetically separated into groups defined by the number of doublons in the given state. Those groups are commonly called Hubbard subbands [41,42,45]. For high U, changes in $D(t)$ therefore also indicate excitation.

We will also benefit from a measure that correlates more directly to the probability of doublon-holon pair creation. With that in mind, we utilize the following measure:

$$P_{af}(t) = \left\langle \sum_{\langle i,j \rangle} \frac{\hat{n}_{\uparrow,i}(\hat{I} - \hat{n}_{\downarrow,i})(\hat{I} - \hat{n}_{\uparrow,j})\hat{n}_{\downarrow,j}}{L} \right\rangle, \quad (9)$$

which gives the probability of observing antiferromagnetic ("af") ordering when observing two neighboring sites at random. Regarding the notation, i and j are nearest-neighbor lattice site indices, denoted by $\langle i, j \rangle$. Note that antiferromagnetic ordering across two sites, depicted as the final configuration in Fig. 1(a) and initial configuration in Fig. 1(b), means there is precisely one electron on each site, and that they have opposite spin. As doublon-holon pairs can only be created through transitions across antiferromagnetically ordered, nearest-neighbor sites, as depicted in Fig. 1(b), the probability of observing sites with antiferromagnetic order is heavily correlated to the probability of doublon-holon-pair-creating transitions.

We will also utilize the Mott gap, which is a jump in the chemical potential around half-filling. Adding an electron to the system when it is less than half-filled does not require the creation of a new doublon. In opposition, a new doublon is created by adding an electron to the system when it is at half-filling or above. This difference means the U term has little to no impact on the chemical potential when adding an electron below half-filling but a substantial impact when adding an electron at or above half-filling. The Mott gap can be calculated as [41,54]

$$\Delta_{Mott}(U) = E_{GS}^{L+1}(U) + E_{GS}^{L-1}(U) - 2E_{GS}^L(U), \quad (10)$$

where $E_{GS}^n(U)$ is the ground-state energy of the system containing n electrons and U being the U value from the Hubbard Hamiltonian (1). Note that $n = L$ corresponds to half-filling. The Mott gap in Eq. (10) is an approximation to the minimum energy needed to create a doublon-holon pair and is calculable without having to diagonalize the entire system. Diagonalization of the entire system is often not tractable due to memory constraints.

Finally, we will need some basic results regarding the Bloch band described by the hopping term in the $U = 0$ limit. In this case, the field-free tight-binding model can be solved analytically for the ground-state energy:

$$E_{GS}^n(U = 0) = 2 \sum_{i=\lceil -\frac{n-1}{4} \rceil}^{\lceil \frac{n-1}{4} \rceil} \epsilon(k_i) \quad (11)$$

$$\epsilon(k_i) = -2t_0 \cos(k_i a), \quad (12)$$

$$k_i = \frac{i2\pi}{La}, \quad i \in \left\{ 0, \pm 1, \dots, \pm\left(\frac{L}{2} - 1\right), \frac{L}{2} \right\}. \quad (13)$$

Here $\epsilon(k_i)$ is the energy of the Bloch state with crystal momentum k_i, and n is the number of electrons in the lattice. We assume here and throughout an equal number of spin-down and spin-up electrons. We write the rounding up operator as the $\lceil \square \rceil$ brackets. The total energy width of the Bloch band, commonly known as its bandwidth, is

$$\Delta_{width} = 4t_0, \quad (14)$$

which corresponds to $\simeq 15$ harmonic orders. In the following we will use the term energy width of the Bloch band to describe Δ_{width} to avoid any confusion with the bandwidth of the laser pulse.

By using the hopping term in Eq. (1) and the Heisenberg equation of motion one can then show that in the $U = 0$ case the current reads as

$$j_0(t) = a E_{\text{GS}}^n(U = 0) \sin[aA(t)], \qquad (15)$$

which shows that for sufficiently small $aA(t)$ the current is directly proportional to the vector potential. Finally, we remark that $E_{\text{GS}}^n(U = 0) < 0$ so positive $A(t)$ yields negative current and vice versa.

III. RESULTS AND DISCUSSION

In this section, we present our results and analyses. We consider four U values: $U = 0.1t_0$, $2t_0$, $5t_0$, and $10t_0$, which are picked as representative values based on a more thorough parameter scan. U values up to $10t_0$ have been seen in cuprates [55].

A. HHG spectra

We begin by discussing the HHG spectra for various U values and degrees of band filling, as shown in Fig. 2. The spectra are identical with respect to band filling around half-filling, which is why only three of the five plotted degrees of band filling are visible in each panel. First, we present some important points from Fig. 2 and leave the discussion of their origin for later to relate those observations to equations from the previous section. We will refrain from introducing a more qualitative picture of the results until later as we will benefit from more results before doing so.

Figures 2(a) and 2(b) show spectra for $U = 0.1t_0$ and $2t_0$, respectively. In both cases, the changing degree of band filling has minimal impact on the spectra. The oscillations in the $U = 0.1t_0$ half-filled lattice spectrum which start from around the 55th harmonic are a result of numerical uncertainty. The spectra for $U = 0.1t_0$ and $2t_0$ are dominated by plateaus ending at approximately the 30th harmonic order. Thirty harmonic orders correspond to twice the energy width of the Bloch band, $2\Delta_{\text{width}}$. As the U term is not diagonal in k space it couples different states in the Bloch bands. This means the U term can move electrons to the peaks of the Bloch band. This means harmonics with energy corresponding to Δ_{width}, approximately the 15th harmonic order, can be created through a single-electron transition. As the U term is a two-particle operator, it can transfer two electrons in k space at any given time. This doubles the maximal energy gap between initial and final states which caps the harmonics at the 30th order. Transitions with higher energy than that are not possible by moving two electrons within the Bloch band, so the emission of harmonics with higher energy than $2\Delta_{\text{width}}$ is unlikely. This is indicated by the plateau ending at approximately 30 harmonic orders in both Fig. 2(a), $U = 0.1t_0$, and 2(b), $U = 2t_0$. For such low U the creation or annihilation of doublons have little to no impact on the energy associated with the transitions and therefore little to no impact on the harmonics generated. For larger U, a relatively larger
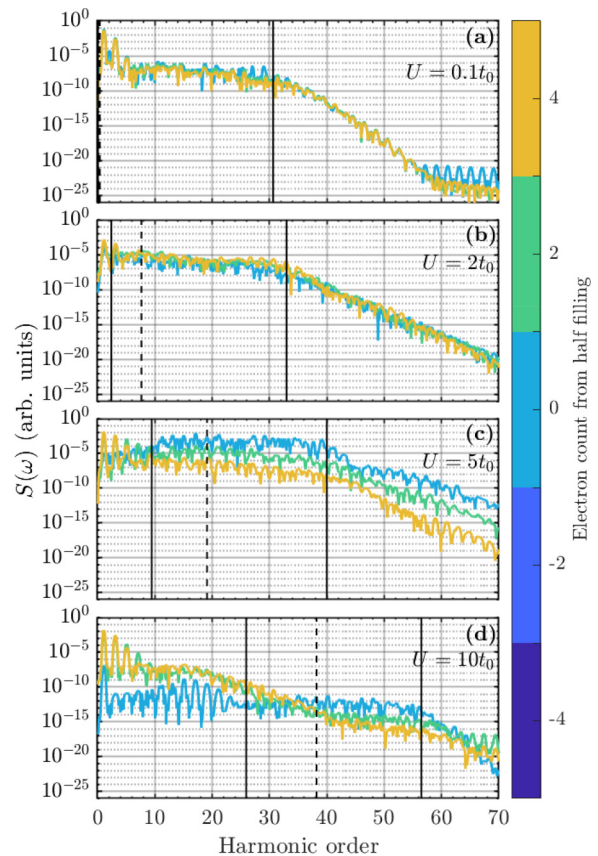

FIG. 2. HHG spectra [Eq. (3)] for different degrees of band filling and Hubbard U. (a) $U = 0.1t_0$, (b) $U = 2t_0$, (c) $U = 5t_0$, and (d) $U = 10t_0$. The dashed, black vertical lines indicate the U value in terms of harmonic orders, the full black vertical lines on the left indicate the Mott gap [see Eq. (10)], and the full black vertical lines on the right indicate the Mott gap plus twice the energy width of the underlying Bloch band, i.e., $\Delta_{\text{Mott}}(U) + 2\Delta_{\text{width}}$.

energy is needed when creating a doublon and likewise a relatively larger energy is released when annihilating a doublon. This means that harmonics with energy below Δ_{Mott} cannot be created from doublon annihilation. Note that the Mott gap increases with U. In both the $U = 0.1t_0$ and $2t_0$ cases the Mott gap is small, $\Delta_{\text{Mott}} = 0.07$ and 2.4 harmonic orders, respectively. For $U = 5t_0$ [Fig. 2(c)], the Mott gap has increased to $\Delta_{\text{Mott}} = 9.4$ harmonic orders, which coincides nicely with the beginning of the observed spectral plateau. The plateau then extends to around the 40th harmonic order resulting in a total plateau length of 30 harmonic orders as for the lower U values. While this looks similarly to the result obtained for lower U, the physical mechanism is likely different as the U term will dominate the electron dynamics in this limit. The most likely mechanism is that a doublon-holon pair is created, propagates in their respective Hubbard subbands before recombining under emission of a harmonic corresponding to the band gap at the recombination point, i.e., inter-Hubbard-subband HHG. As the Hubbard subbands are expected to have approximately the same bandwidth as the Bloch band, that mechanism will create a plateau like the one observed. For $U = 10t_0$ [Fig. 2(d)] a similar plateau can be seen from the half-filled lattice. The plateau stretches

from $\Delta_{\mathrm{Mott}} \simeq 25.9$ harmonic orders to around 56 harmonic orders, i.e., again by twice the energy width of the Bloch band $2\Delta_{\mathrm{width}}$ [see the full black lines in Fig. 2(d)]. This plateau has dropped by around nine orders of magnitude, compared with the plateau for $U = 5t_0$ [Fig. 2(c)]. This drop is due to the substantially increased U value and therefore increased Δ_{Mott}. This increase means that it requires significantly more energy to create a doublon-holon pair which makes the creation of such pairs significantly less likely. In the doped cases there does not seem to be a plateau starting from Δ_{Mott} in Fig. 2(d) where $U = 10t_0$. This is due to the higher-lying plateau which starts its dropoff at around the 15th harmonic order. The signal from this plateau does not drop to the level of the other plateau before around the 35th harmonic order, at which point a second plateau begins. Note that this second plateau decreases with increasing doping rate. This second plateau ends at approximately $\Delta_{\mathrm{Mott}} + 2\Delta_{\mathrm{width}}$ and is therefore likely a U-induced plateau like the ones described for the lower $U = 0.1t_0$, $2t_0$, and $5t_0$ values. The origin of the high-lying plateau extending to around the 15th harmonic order in Fig. 2(d) is believed to be hopping of doublons and holons, as it cannot be annihilation of doublons as the harmonics are well below Δ_{Mott}.

We finally note that the results observed here for $U = 10t_0$ are in line with results observed experimentally from single-wall carbon nanotubes in a semiconductor regime [56] and theoretically from doped band-gap materials [57] in the following sense. In those references, doping was observed to increase the spectral gain for low-harmonic orders but to decrease it for high-harmonic orders. Beyond that it was found that interband dynamics, i.e., transitions from one Bloch band to another, is the dominating source of HHG above the band gap whereas intraband dynamics, i.e., transitions within a given Bloch band, dominate below the band gap. Here, for $U = 10t_0$, we observe similar results in the setting of a correlated system in the following sense. Below Δ_{Mott}, there is a clear enhancement of the HHG spectra from doping by around five orders of magnitude. This enhancement is so significant that the doped systems continue to show an overall enhancement even beyond $\Delta_{\mathrm{Mott}} \simeq 26$ harmonic orders. However, after around 35 harmonic orders the signals from the doped systems have dropped off below the signal of the undoped system. From then on there is a clear difference in the height of the plateaus, ordered by the degree of doping, so the undoped system yields around five orders of magnitude more HHG than the doped systems. Treating Δ_{Mott} as the band gap yields a parallel between intraband and interband current and the $j_{\mathrm{hop}}(t)$ and $j_{\mathrm{ca}}(t)$ introduced in Sec. II. The hopping current $j_{\mathrm{hop}}(t)$ does not include transitions which change the number of doublon-holon pairs in the state. The current $j_{\mathrm{hop}}(t)$ is therefore strictly an intra-Hubbard-subband current, and a parallel to an intraband current. Similarly, $j_{\mathrm{ca}}(t)$ describes transitions which change the number of doublon-holon pairs and is therefore an inter-Hubbard-subband current. We will discuss this parallel further in later sections.

B. Total current results

To provide further insight into the spectral changes displayed in Fig. 2, we show, in Fig. 3, the currents used to
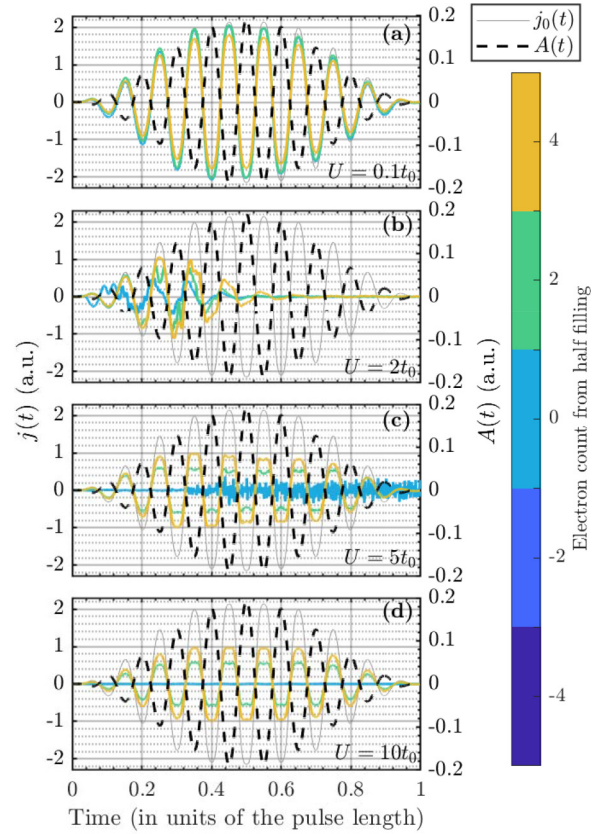

FIG. 3. The current generated via Eq. (4), for different degrees of band filling and Hubbard U. (a) $U = 0.1t_0$, (b) $U = 2t_0$, (c) $U = 5t_0$, and (d) $U = 10t_0$. In all panels the vector potential is shown by the dashed, black line and the Bloch current from the half-filled lattice $j_0(t)$ [Eq. (15)] is shown via the thin, gray line.

generate the spectra. The increasing importance of the degree of band filling as U increases, observed in Fig. 2, holds here too. In Fig. 3(a), where $U = 0.1t_0$, the degree of band filling has little impact. This is consistent with the analytical result which is derivable for $U = 0$ where the Hubbard model reduces to a tight-binding model. This tight-binding model can be solved by employing Bloch's theorem resulting in the current given by Eq. (15), which is in line with observed results.

For $U = 2t_0$ [Fig. 3(b)], the differences between the currents for different doping levels are larger, but still show similar behavior in terms of a drop to approximately zero halfway through the simulation, which is consistent with earlier results [32].

At higher U, the half-filled band behaves markedly different from the others. For $U = 5t_0$ [Fig. 3(c)], the half-filled current oscillates at a much higher rate than the non-half-filled bands and rises in amplitude as the pulse amplitude increases. Furthermore, the current for the half-filled band does not decrease at the end of the pulse. For the even higher U of Fig. 3(d), $U = 10t_0$, the current from the half-filled lattice has decreased to order 10^{-3} a.u., which is practically indistinguishable from 0 in the figure. In contrast to this, the non-half-filled lattices display currents largely similar to the $U \approx 0$ currents, the most notable difference being that

the peak amplitude has decreased by a factor of ≈ 2 when comparing $U = 0.1t_0$ and $10t_0$.

C. Qualitative description of the dynamics

Our understanding of the observations from Figs. 2 and 3 is best formulated in the quasiparticle picture of doublons and holons. The U term of the Hubbard model punishes the creation of doublons energetically. Therefore, the ground state mainly includes the configurations with minimal doublon count. For the half-filled lattice, this means the ground state is dominated by configurations that have one electron on each site. Any electron hopping, from such configurations, will result in the creation of a doublon-holon pair. Thus, virtually no dynamics can be induced from the ground state without the creation of a doublon-holon pair. For high U this results in two effects. First, the current amplitude decreases significantly because transport is impeded by the cost in energy, $\Delta_{\text{Mott}}(U)$, associated with the creation of a doublon-holon pair. Second, the spectra lose gain below Δ_{Mott}, but gain intensity above it, as can be seen in Fig. 2(d).

If the band is not half-filled, all configurations will necessarily have one or more doublon(s) or holon(s). Therefore, electrons can move about the lattice without creating doublon-holon pairs, at no energy cost, thus enabling dynamics even in the high-U limit [see Fig. 3(d)]. Note that in dimensions higher than one, the movement of doublons or holons will result in spin frustrations of the lattice. The movement of doublons and holons will therefore have some associated energy cost. This energy cost originates from the hopping term and is therefore related to the t_0 value, which is small compared to U for highly correlated materials. Spin dynamics have very recently been observed to impact the HHG spectrum from highly correlated materials [35,36]. For large U, the creation and annihilation of doublon-holon pairs is associated with large energy transitions and therefore with truly high-order harmonics, as will be demonstrated in further detail later.

D. Doublon and holon measures

In this section, we utilize the measures of Eqs. (8) and (9) to gain further understanding of the doublon-holon pair creation and annihilation throughout the simulation.

1. D measure

Figure 4 shows $D(t)$ [see Eq. (8)] for different degrees of band filling and U. We note immediately from all panels that removing or adding electrons to the lattice will change the number of doublons in the lattice. To estimate the impact of varying band filling on $D(t)$ we calculated the D measure from the state in which every possible electron configuration is equally likely. In this case, the D measure equals $n_\uparrow n_\downarrow / L^2$, where $n_\uparrow$ and $n_\downarrow$ are the number of electrons in the lattice with spin up and down, respectively. Note that $n_\uparrow / L$ gives the probability that an arbitrarily picked site contains a spin-up electron and similarly for spin down, so their product gives the probability of observing a doublon, i.e., for the site to have both a spin-up and -down electron. This resulted in the following values, with four electrons removed from half-filling: $D = \frac{1}{9} \simeq 0.111$, with two electrons removed $D = \frac{25}{144} \simeq 0.174$,
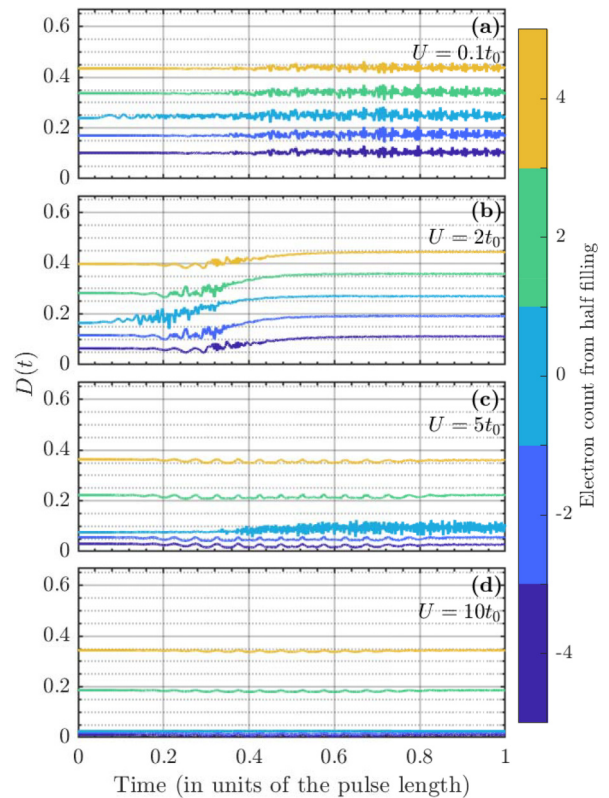

FIG. 4. The D measure of Eq. (8) for different degrees of band filling and Hubbard U. (a) $U = 0.1t_0$, (b) $U = 2t_0$, (c) $U = 5t_0$, and (d) $U = 10t_0$.

at half-filling $D = \frac{1}{4} = 0.25$, with two electrons added $D = \frac{49}{144} \simeq 0.340$, and with four electrons added $D = \frac{4}{9} \simeq 0.444$. In Fig. 4(a) the D measure is plotted for $U = 0.1t_0$. The D values are close to constant and very close to the values given above for equal probability of all electron configurations. This makes sense as for $U \ll t_0$ the system's eigenvalues are close to the Bloch states, which are the eigenstates for $U = 0$. The Bloch states are completely localized in k space, so therefore completely delocalized in real space. This delocalization causes each electron configuration to be approximately equally probable. We note from Figs. 4(b)–4(d) that the initial ground state has decreasing D values with increasing U and below the values from states with equal probability of all electron configurations. This is a result of the increasing energetic cost to create doublons. Minimizing the energy of the state implies minimizing the number of doublons, and therefore the probability of observing configurations with a high number of doublons. In Fig. 4(b), with $U = 2t_0$, there is a noticeable increase in the D values over the time interval 0.2–0.5 pulse lengths. This increase is not present for lower- or higher-U values. This can be explained by considering the correlation between the number of doublons in and the energy of a given state, as well as general features of the energy spectrum. For low U the energy of a state is largely determined by the hopping term of the Hamiltonian [Eq. (1)], whereas for higher U it is determined by the U term. As mentioned, Bloch states, the eigenstates of the hopping term, are delocalized in real space and, as a result, there is little to no correlation between the

energy and the number of doublons in the state. On the other hand, the expectation value of the U term depends only on the U value and the number of doublons in the state, resulting in complete correlation between the number of doublons in the state and the energy from the U term. This means for low $U = 0.1t_0$, exciting the system, i.e., increasing the energy of the system, does not increase the number of doublons in the state, causing D to remain virtually constant. This explains why D is approximately constant in Fig. 4(a). For higher U [see Figs. 4(c) and 4(d) with $U = 5t_0$ and $10t_0$, respectively], the D values are also approximately constant, despite the high degree of correlation between the energy and doublon count. This can be understood by considering the energy gaps between the eigenvalues of the system. For $U = 0$ many of the states are highly degenerate; see Ref. [32] for a discussion. That degeneracy is removed when U becomes nonzero. As U increases further the energy gaps between the states increase steadily, resulting in relatively large energy gaps. Since the pulse used is the same throughout this work, the degree of system excitation decreases as U increases. So due to the minimal degree of excitation, the D values change minimally in both Figs. 4(c) and 4(d), despite the correlation between energy and D value.

For $U \rightarrow \infty$, the D measure attains the value corresponding to the configurations with the minimal number of doublons. If the lattice is half-filled or less, then there is at minimum one site per electron and $D = 0$, i.e., states with no doublons, can be achieved. When the lattice is more than or half-filled, each added electron adds another doublon, causing an increase in D of $\frac{1}{L} \simeq 0.083$. This is in line with the D values of Figs. 4(c) and 4(d). Finally, we note that the oscillations observed in the D values of Figs. 4(c) and 4(d) reach a local maximum when the electric field from the pulse (not shown) peaks, i.e., when the rate of excitation is maximal.

2. P_{af} measure

Here we discuss the P_{af} measure of Eq. (9), which is shown in Fig. 5. As P_{af} is heavily dependent on the number of electrons in the lattice it can be difficult to compare P_{af} values for different degrees of band filling. In order to give an idea of those changes in the P_{af} values, we give the P_{af} values for states with equal probability of observing each electron configuration. At half-filling $P_{af} \simeq 0.149$, with two electrons added or removed from half-filling $P_{af} \simeq 0.141$, and with four electrons added or removed from half-filling $P_{af} \simeq 0.118$. First, we note that the P_{af} values are virtually constant at all times for $U = 0.1t_0$, $U = 5t_0$, and $U = 10t_0$ [Figs. 5(a), 5(c), and 5(d), respectively]. This is for the same reasons as those explaining the equivalent observation on the D values, presented in Sec. III D 1, i.e., due to a low correlation between the energy, doublon count, and antiferromagnetic ordering in the initial ground state for low U, and large energy gaps between the eigenstates, leading to a low degree of excitation, for high U. We note, however, that the P_{af} values decrease in Fig. 5(b), simultaneously with the increase in D values, between 0.2 and 0.5 pulse lengths. We understand the decrease in terms of the increasing number of doublons resulting in fewer electrons and sites having the possibility of being antiferromagnetically ordered, thus decreasing P_{af}.
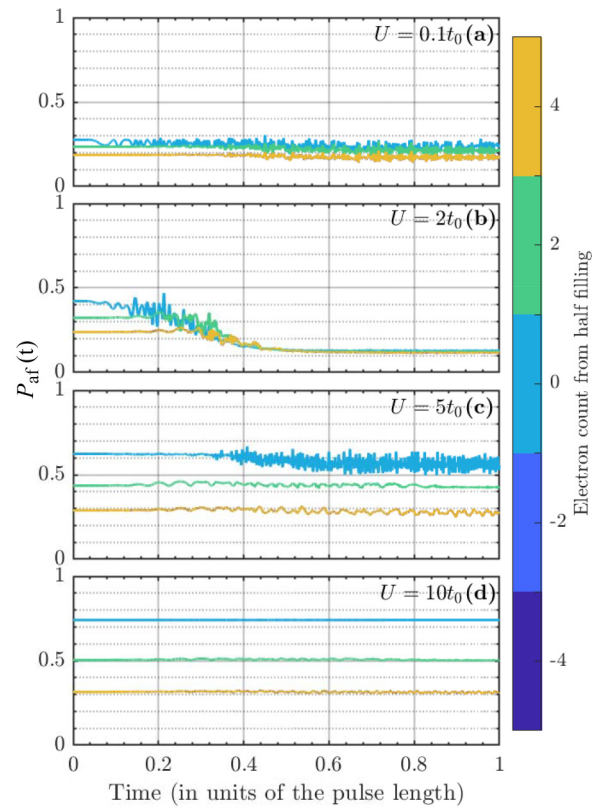

FIG. 5. The P_{af} measure of Eq. (9), for different degrees of band filling and Hubbard U. (a) $U = 0.1t_0$, (b) $U = 2t_0$, (c) $U = 5t_0$, and (d) $U = 10t_0$.

3. Summary regarding the D and P_{af} measures

We conclude from the observations of the previous two subsections that for low U, i.e., $U = 0.1t_0$, doublon-holon pairs are being created and annihilated, but as there is little energy involved with this process, the rates of creation and annihilation are very close to equal. We note also, based on the low-P_{af} values [see Fig. 5(a)], that the creation and annihilation of doublon-holon pairs correspond to a smaller portion of the dynamics than for higher U. For higher U, i.e., $U = 5t_0$ and $10t_0$, the system is less dynamical overall, as indicated by the currents shown in Fig. 3. The higher P_{af} seen in Fig. 5(d) and increasing weakly oscillating D measure [see between the times 0.2 and 0.8 pulse lengths in Fig. 4(d)] indicates that doublon-holon-pair-creating or -annihilating transitions are more prevalent. As U becomes significantly larger than t_0 the interpretation of the results begins to depend significantly on the degree of band filling. In the half-filled case there are virtually no dynamics left in the system, but the transitions that do happen are virtually exclusively of the doublon-holon pair creating or annihilating type. Whereas for the non-half-filled lattices the existence of either doublons or holons in the ground state implies that transitions at no U-induced energy cost are possible. Such transitions may allow the electrons to build up momentum before interacting with other electrons. The increased energy associated with the buildup of momentum increases the probability of such interactions, resulting in the creation of a doublon-holon pair. The existence of doublons or holons in every electron configuration means it
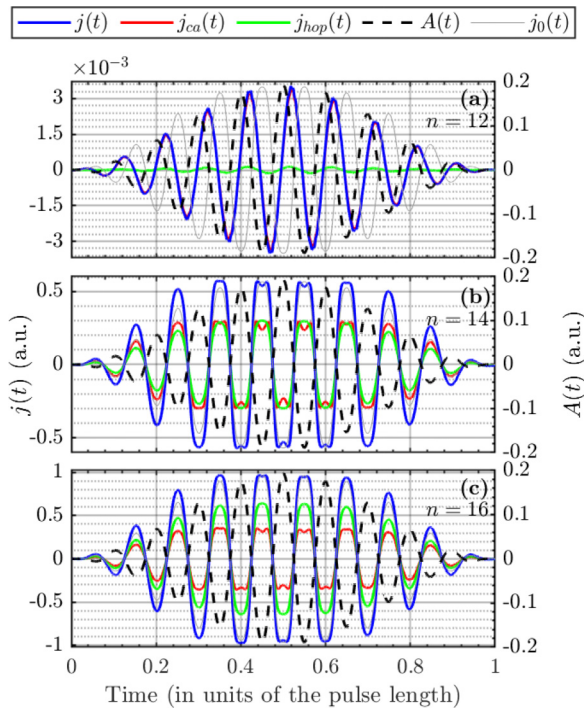
FIG. 6. The creation and annihilation current $j_{ca}(t)$ from Eq. (5), and the hopping current $j_{hop}(t)$ from Eq. (6), for the $U = 10t_0$ system for lattices with n electrons. Half-filling corresponds to $n = L = 12$. The total current is shown by the full, blue curve and the vector potential is shown by the black, dashed line. Finally, the scaled down Bloch current is shown by the thin, gray line. The scaling factors are given by $\max[|j(t)|]/|2aE_{GS}|$, (a) $\simeq 1.9 \times 10^{-3}$, (b) $\simeq 0.31$, (c) $\simeq 0.52$. Note that in (a), $j_{ca}(t)$ is identical to the total current $j(t)$ on the scale of the figure.

is easier for the laser pulse to generate doublon or holon hopping and thereby generate low-harmonic orders as can be seen in Fig. 2(d) where $U = 10t_0$. It also means a lower P_{af} value [see Fig. 5(d)], which means less doublon-holon pair generation and therefore less inter-Hubbard-subband HHG. As we shall now see all of the conclusions and indications in this section are consistent with behavior of the currents $j_{ca}(t)$ and $j_{hop}(t)$ and the associated spectra.

E. Quasiparticle currents

To support the explanation of Sec. III C, regarding doping effects on the dynamics, and verify the points from Sec. III D 3, we show $j_{ca}(t)$ [Eq. (5)] and $j_{hop}(t)$ [Eq. (6)] for $U = 10t_0$ in Fig. 6. We only plot the currents for lattices which are at least half-filled, due to the earlier mentioned symmetry, and only consider $U = 10t_0$ as the U value needs to be significantly larger than Δ_{width} in order for the doublon-holon picture to capture the physics. In Fig. 6(a) the currents in the half-filled lattice are shown. We note that the majority of the current arises from the creation or annihilation of doublon-holon pairs $j_{ca}(t)$. This finding is consistent with the explanation described above, as for $U = 10t_0$ the ground state will be dominated by the antiferromagnetically ordered, doublon-holon-pair-free configurations. From such configurations any electron hopping will lead to the creation of a

doublon-holon pair. That is unlikely due to the associated energy cost U. Note also that, in this case, the current is only of order 10^{-3} a.u. For a lattice with 14 electrons [Fig. 6(b)], the current arising from the hopping of the doublons and holons approximately equals the current arising from creation or annihilation of said quasiparticles. It is worth noting that with 14 electrons in the lattice the ground state is dominated by configurations with 2 doublons. This means there are significantly more ways for an electron to hop resulting in the creation of a doublon-holon pair than in a doublon hopping. Figure 5 verifies this by showing that the probability of observing antiferromagnetic ordering is consistently higher for states with two electrons added relative to half-filling compared with the probability for observing antiferromagnetic ordering from half-filled states from an even probability of all configurations, i.e., P_{af} is consistently larger than 0.141. Note that the result of annihilating a doublon-holon pair is antiferromagnetic ordering, and inversely that antiferromagnetic ordering is needed to facilitate doublon-holon-pair-creating transitions (see Fig. 1). The currents in Fig. 6 are all for $U = 10t_0$ corresponding to Fig. 5(d). We note from Fig. 5 that the probability of observing antiferromagnetic ordering generally increases with U. That trend is reasonable since antiferromagnetically ordered configurations do not contain doublons and the impact on P_{af} of removing or adding electrons to the lattice increases similarly, as seen from the sizes of the gaps between the lines in Fig. 5. If there are more possible transitions from the ground state that may result in the creation of a doublon-holon pair, than transitions which move doublons or holons, then everything else being equal, $j_{ca}(t) > j_{hop}(t)$. So that $j_{ca}(t) \approx j_{hop}(t)$, for this lattice, indicates that hopping transitions are more likely than creation or annihilation transitions relative to the number of lattice gaps that enable the given type of transition.

With 16 electrons in the lattice [Fig. 6(c)], the hopping current is larger than the creation or annihilation current at all times, consistent with the larger number of doublons in the ground state. Noting the parallel between $j_{hop}(t)$ and $j_{ca}(t)$ to intraband and interband currents, similar scaling between the mechanisms has been observed from single-wall carbon nanotubes [56] and doped band-gap materials [57].

We note that the currents in Fig. 6(a) are out of phase with the Bloch current $j_0(t)$ [Eq. (15)]. The currents peak when the electric field peaks, instead of when the vector potential peaks. That is because the ground state is dominated by the antiferromagnetically ordered electron configurations. Any transition from such a configuration results in the creation of a doublon-holon pair, which, for high U, is most likely at high laser intensity, and therefore peak electric field. Inversely, the currents in the non-half-filled lattices are in phase with the Bloch current. That is due to the free electrons associated with the ever-present doublons or holons which, qualitatively, are Bloch type, i.e., free to move about the lattice, and only interacting with other particles via Pauli's exclusion principle.

Finally, we note that the current amplitude scales approximately linearly with the number of electrons added or removed from the lattice relative to half-filling, i.e., with the number of free carriers in the form of doublons or holons. This scaling is consistent with the Drude model.
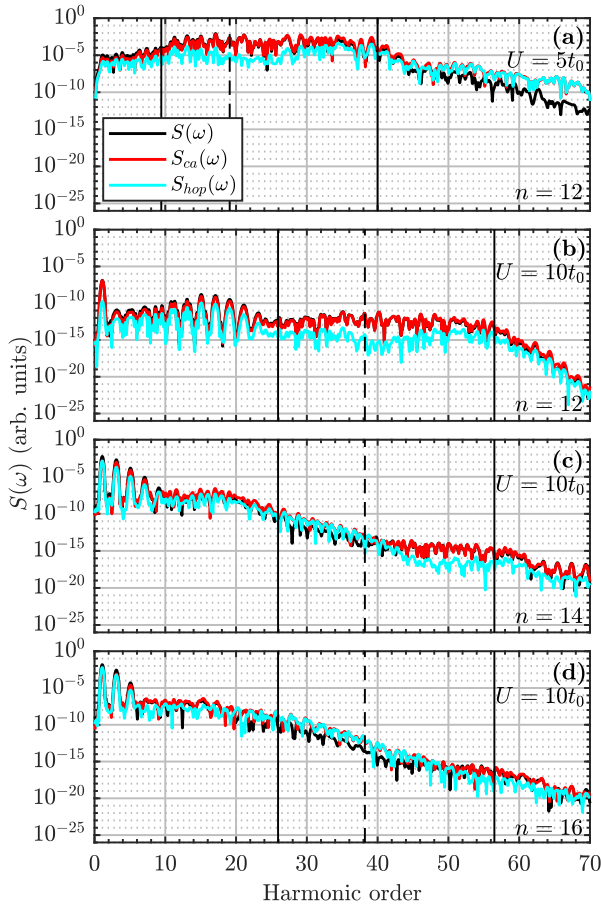
FIG. 7. The creation and annihilation $S_{ca}(\omega)$ and hopping $S_{hop}(\omega)$ spectra [Eq. (7)] from lattices with various values of U: (a) $U = 5t_0$, (b) $U = 10t_0$, (c)–(e) $U = 10t_0$, and degrees of band filling (a)–(c) $n = 12$, (d) $n = 14$, and (e) $n = 16$. The dashed, black vertical lines indicate the U value in terms of harmonic orders, the full black lines on the left indicate the Mott gap in terms of harmonic orders, and the full black lines on the right indicate the Mott gap plus two times the energy width of the Bloch band.

F. Quasiparticle spectra

In order to obtain more insight into the link between the two types of dynamics associated with $\hat{j}_{ca}(t)$ [Eq. (5)] and $\hat{j}_{hop}(t)$ [Eq. (6)], we show spectra generated from each current type alone in Fig. 7. We note that the sum of the spectra from these two currents neither does nor should add up to the spectrum generated from the total current due to interference terms from the norm-square in Eq. (3); see text after Eq. (7). It is, however, still reasonable to expect that general trends concerning which harmonics are generated from which mechanism can be gleaned from this analysis.

For $U = 5t_0$ [Fig. 7(a)], $S_{ca}(\omega)$ is multiple orders of magnitude higher, than $S_{hop}(\omega)$, between Δ_{Mott} and $\Delta_{Mott} + 2\Delta_{width}$. That is likely a result of the high number of transitions from the dominating antiferromagnetically ordered configuration which can only result in the production of doublon-holon pairs. Such transitions will inevitably result in the generation of harmonics with energy above Δ_{Mott}. For $U = 10t_0$ [Fig. 7(b)], $S_{ca}(\omega)$ is larger than $S_{hop}(\omega)$ across the entire spectrum, but the difference is largest for harmonic orders 26–56,

which correspond to Δ_{Mott} to $\Delta_{Mott} + 2\Delta_{width}$. It makes sense that $S_{ca}(\omega)$ dominates in that region as the plateau is generated from the annihilation of doublon-holon pairs as described earlier. When doping is introduced, the plateau becomes harder to see as described earlier. This means the enhancement in the inter-Hubbard-subband plateau also becomes harder to see. However, it is still visible in Fig. 7(c) between the 40th and 60th harmonic orders, which overlaps with the area in which the corresponding plateau is visible in Fig. 2(d). In Fig. 7(d) the end of the plateau is visible between the 50th and 60th harmonic orders, which is also in agreement with the plateau seen in Fig. 2(d). Throughout all spectra, even outside the plateau regions, in Fig. 7, $S_{ca}(\omega) \gtrsim S_{hop}(\omega)$. As the ground state is dominated by the antiferromagnetically ordered configurations in all the plotted cases, the majority of the dynamics from the initial state will be of the creating type which causes $S_{ca}(\omega)$ to dominate. Note also how that domination decreases outside of the plateau regions as the degree of doping increases. This can be seen from the decreasing difference between $S_{ca}(\omega)$ and $S_{hop}(\omega)$ for harmonic orders outside the plateau region, e.g., less than 15. While $S_{ca}(\omega)$ and $S(\omega)$ agree quite closely in the Mott-insulator limit [Fig. 7(b)], we observe some degree of deviation as doping in increased [see Figs. 7(c) and 7(d)]. This means that the interference between the hopping and creation and annihilation currents increases and has to be taken into account to describe $S(\omega)$. This is in line with the observed increasing importance of $j_{hop}(t)$ in Fig. 6. Therefore, in the Mott-insulating limit, i.e., in the high-U and undoped cases, the creation and annihilation dynamics captures all the dynamics in the system rather well; see also Refs. [23,24]. However, outside of the Mott-insulating limit, whether that be by lower U [Fig. 7(a)] or doping away from half-filling, creation and annihilation dynamics do not appear to capture the total dynamics, as indicated in Fig. 6, and in Fig. 7 by the decreasing agreement between $S_{ca}(\omega)$ and $S(\omega)$.

IV. SUMMARY AND CONCLUSION

In this work, we have used the Hubbard model to study HHG beyond the assumption of half-filling, corresponding to a situation where the correlated material is doped. We have done this to begin answering how HHG operates from highly doped and correlated materials. In previous studies of HHG using the Hubbard model for the half-filled case, it was shown that increasing the Hubbard U leads to increased gain in the HHG spectra for $U \leqslant 5t_0$ [10]. On top of that, a parallel to the three-step model was developed in the half-filled case based on the creation and annihilation of doublons and holons [24]. With these facts in mind, we set out to answer the following questions: (i) What effects does doping have on the HHG spectra? (ii) How do the dynamics of non-half-filled bands differ from half-filled bands? (iii) How do the changes in the dynamics and HHG spectra relate to one another? It was found that going beyond half-filling has little to no effect on the spectra for low U, but that for higher U there are marked differences. For $U = 5t_0$ the half-filled lattice showed significantly higher high-harmonic gain than the non-half-filled lattices, particularly in the region between Δ_{Mott} and $\Delta_{Mott} + 2\Delta_{width}$. For higher U the half-filled lattice dropped to be the lattice with least harmonic gain for low to medium-harmonic

orders but still gave the highest gain for high-harmonic orders. This finding may be rationalized in terms of the high energy needed to produce doublon-holon pairs. We explained this by splitting the dynamics into two mechanisms: (i) movement of the doublons or holons, the parallel to intraband dynamics, and (ii) creation and annihilation of doublon-holon pairs, the parallel to interband dynamics. For high-U values the ground state of the Hubbard model is dominated by the configurations with the highest probability of observing antiferromagnetic ordering (see Fig. 5). For half-filling this results in every hop of the electrons creating a doublon-holon pair. For high U, this pair creation requires a lot of energy, resulting in minimal dynamics and thus minimal harmonic gain. For lower U, the lower-energy cost of creating a doublon-holon pair means that relatively more dynamics associated with the creation and annihilation of doublon-holon pairs take place. When the lattice is not half-filled, all configurations, and by extension, the ground state will contain either doublons or holons. As a result, regardless of the size of the U term, dynamics associated with the movement of doublons or holons can take place at no extra U-induced energy cost. This absence of an energy penalty results in the spectra being significantly less affected by the U term and, as a result, higher-harmonic gain in the high-U limit compared with the half-filled case was observed below the Mott gap. For harmonic orders above the Mott gap, the presence of doublons or holons in all configurations of the doped systems makes doublon-holon pair creation less likely than in the half-filled case. This results in lower inter-Hubbard-subband gain and therefore lower HHG signal than in the nondoped case. We substantiated this explanation by investigating the currents associated with the two mechanisms in the high-U limit. In the half-filled case, there is significantly less current than in the non-half-filled cases, and it is dominated by the creation and annihilation current. In the non-half-filled cases, the current associated with the movements of the doublons or holons becomes increasingly important, with the total current rising in amplitude accordingly. We analyzed spectra generated from the hopping and creation and annihilation currents only. We found that in the half-filling case, increasing U leads to the majority of the spectral gain being formed through creation and annihilation dynamics. We further identified a plateau between Δ_{Mott} and $\Delta_{\text{Mott}} + 2\Delta_{\text{width}}$, which we explain through the ability of the U terms to take two electrons from the peak to the bottom of the Bloch band described by the hopping term. In this region of the spectrum it was found that creation and annihilation of doublon-holon pairs is giving the dominating contribution to the HHG. We explain this via the earlier mentioned parallel to the interband and intraband-based three-step model.

In conclusion, this study shows that the degree of band filling is of immense importance to the gain in HHG for highly correlated materials. In cases with doping away from the half-filling situation, the doping-induced enhancement of the HHG spectra extends to the lowest harmonic orders and can be enhanced by as much as 10 orders of magnitude. The significant enhancement is a very clear signature of the sensitive, ultrafast response of correlated electron dynamics to extreme nonperturbative driving by intense laser pulses.

This work focused on effects of doping on HHG from highly correlated systems. As such, it raises a number of interesting future research questions. Some of these relate to the approximations introduced in dealing with the numerical scaling of the Hubbard model, e.g., the lattice size and dimensionality, the single Bloch-band approximation, and including only hopping and onsite interactions. Going beyond these approximations would allow elucidation of surface effects on HHG, of the interplay between interband dynamics in the Bloch picture, and the correlated creation-annihilation dynamics of doublon-holon pairs. In particular, the one-dimensional description used in this study means that when two electrons meet they can only pass one another by creating a doublon. In two or three dimensions this is not so. It may also be of interest to look at the effects of doping on the spin and spinon dynamics and its potential impact on the HHG spectra, particularly with the recent results on spin-charge coupling and its significant effect on the HHG spectra in mind [35,36]. Such studies would likely require including a spin-spin interaction to the Hamiltonian. Another topic concerns the study of doping effects on the dispersion of the doublon and holon quasiparticles, and its relation to the HHG spectra. One might be able to gain insight into that dispersion from the currents in the system, especially the $j_{\text{hop}}(t)$ as it relates directly to the movement of quasiparticles through the system.

[1] O. Schubert, M. Hohenleutner, F. Langer, B. Urbanek, C. Lange, U. Huttner, D. Golde, T. Meier, M. Kira, S. W. Koch, and R. Huber, Sub-cycle control of terahertz high-harmonic generation by dynamical Bloch oscillations, Nat. Photonics **8**, 119 (2014).

[2] M. Lewenstein, P. Balcou, M. Y. Ivanov, A. L'Huillier, and P. B. Corkum, Theory of high-harmonic generation by low-frequency laser fields, Phys. Rev. A **49**, 2117 (1994).

[3] M. Lein and J. M. Rost, Ultrahigh Harmonics from Laser-Assisted Ion-Atom Collisions, Phys. Rev. Lett. **91**, 243901 (2003).

[4] W. Li, X. Zhou, R. Lock, S. Patchkovskii, A. Stolow, H. C. Kapteyn, and M. M. Murnane, Time-resolved dynamics in probed using high harmonic generation, Science **322**, 1207 (2008).

[5] S. Ghimire, A. D. DiChiara, E. Sistrunk, P. Agostini, L. F. DiMauro, and D. A. Reis, Observation of high-order harmonic generation in a bulk crystal, Nat. Phys. **7**, 138 (2011).

[6] M. Lein, N. Hay, R. Velotta, J. P. Marangos, and P. L. Knight, Interference effects in high-order harmonic generation with molecules, Phys. Rev. A **66**, 023805 (2002).

[7] R. Torres, N. Kajumba, J. G. Underwood, J. S. Robinson, S. Baker, J. W. G. Tisch, R. de Nalda, W. A. Bryan, R. Velotta, C. Altucci, I. C. E. Turcu, and J. P. Marangos, Probing Orbital Structure of Polyatomic Molecules by High-Order Harmonic Generation, Phys. Rev. Lett. **98**, 203007 (2007).

[8] P. M. Kraus, B. Mignolet, D. Baykusheva, A. Rupenyan, L. Horný, E. F. Penka, G. Grassi, O. I. Tolstikhin, J. Schneider, F. Jensen, L. B. Madsen, A. D. Bandrauk, F. Remacle, and H. J. Wörner, Measurement and laser control of attosecond charge migration in ionized iodoacetylene, Science **350**, 790 (2015).

[9] T. T. Luu and H. J. Wörner, Measurement of the Berry curvature of solids using high-harmonic spectroscopy, Nat. Commun. **9**, 916 (2018).

[10] R. E. F. Silva, I. V. Blinov, A. N. Rubtsov, O. Smirnova, and M. Ivanov, High-harmonic spectroscopy of ultrafast many-body dynamics in strongly correlated systems, Nat. Photonics **12**, 266 (2018).

[11] D. Golde, T. Meier, and S. W. Koch, High harmonics generated in semiconductor nanostructures by the coupled dynamics of optical inter- and intraband excitations, Phys. Rev. B **77**, 075330 (2008).

[12] G. Vampa, C. R. McDonald, G. Orlando, D. D. Klug, P. B. Corkum, and T. Brabec, Theoretical Analysis of High-Harmonic Generation in Solids, Phys. Rev. Lett. **113**, 073901 (2014).

[13] M. Garg, M. Zhan, T. T. Luu, H. Lakhotia, T. Klostermann, A. Guggenmos, and E. Goulielmakis, Multi-petahertz electronic metrology, Nature (London) **538**, 359 (2016).

[14] T. T. Luu, M. Garg, S. Y. Kruchinin, A. Moulet, M. T. Hassan, and E. Goulielmakis, Extreme ultraviolet high-harmonic spectroscopy of solids, Nature (London) **521**, 498 (2015).

[15] Y. S. You, D. A. Reis, and S. Ghimire, Anisotropic high-harmonic generation in bulk crystals, Nat. Phys. **13**, 345 (2017).

[16] K. Kaneshima, Y. Shinohara, K. Takeuchi, N. Ishii, K. Imasaka, T. Kaji, S. Ashihara, K. L. Ishikawa, and J. Itatani, Polarization-Resolved Study of High Harmonics from Bulk Semiconductors, Phys. Rev. Lett. **120**, 243903 (2018).

[17] H. Liu, Y. Li, Y. S. You, S. Ghimire, T. F. Heinz, and D. A. Reis, High-harmonic generation from an atomically thin semiconductor, Nat. Phys. **13**, 262 (2017).

[18] S. V. B. Jensen and L. B. Madsen, Propagation time and nondipole contributions to intraband high-order harmonic generation, Phys. Rev. A **105**, L021101 (2022).

[19] S. Yamada and K. Yabana, Determining the optimum thickness for high harmonic generation from nanoscale thin films: An ab initio computational study, Phys. Rev. B **103**, 155426 (2021).

[20] K. K. Hansen, T. Deffge, and D. Bauer, High-order harmonic generation in solid slabs beyond the single-active-electron approximation, Phys. Rev. A **96**, 053418 (2017).

[21] N. Tancogne-Dejean, O. D. Mücke, F. X. Kärtner, and A. Rubio, Impact of the Electronic Band Structure in High-Harmonic Generation Spectra of Solids, Phys. Rev. Lett. **118**, 087403 (2017).

[22] I. Floss, C. Lemell, G. Wachter, V. Smejkal, S. A. Sato, X.-M. Tong, K. Yabana, and J. Burgdörfer, Ab initio multiscale simulation of high-order harmonic generation in solids, Phys. Rev. A **97**, 011401(R) (2018).

[23] Y. Murakami, M. Eckstein, and P. Werner, High-Harmonic Generation in Mott Insulators, Phys. Rev. Lett. **121**, 057405 (2018).

[24] Y. Murakami, S. Takayoshi, A. Koga, and P. Werner, High-harmonic generation in one-dimensional Mott insulators, Phys. Rev. B **103**, 035110 (2021).

[25] Y. Murakami and P. Werner, Nonequilibrium steady states of electric field driven Mott insulators, Phys. Rev. B **98**, 075102 (2018).

[26] M. Lysne, Y. Murakami, and P. Werner, Signatures of bosonic excitations in high-harmonic spectra of Mott insulators, Phys. Rev. B **101**, 195139 (2020).

[27] N. Tancogne-Dejean, M. A. Sentef, and A. Rubio, Ultrafast modification of Hubbard U in a strongly correlated material: Ab initio high-harmonic generation in NiO, Phys. Rev. Lett. **121**, 097402 (2018).

[28] S. Imai, A. Ono, and S. Ishihara, High Harmonic Generation in a Correlated Electron System, Phys. Rev. Lett. **124**, 157404 (2020).

[29] K. Chinzei and T. N. Ikeda, Disorder effects on the origin of high-order harmonic generation in solids, Phys. Rev. Res. **2**, 013033 (2020).

[30] C. Orthodoxou, A. Zaïr, and G. H. Booth, High harmonic generation in two-dimensional Mott insulators, npj Quantum Mater. **6**, 76 (2021).

[31] C. Shao, H. Lu, X. Zhang, C. Yu, T. Tohyama, and R. Lu, High-Harmonic Generation Approaching the Quantum Critical Point of Strongly Correlated Systems, Phys. Rev. Lett. **128**, 047401 (2022).

[32] T. Hansen, S. V. B. Jensen, and L. B. Madsen, Correlation effects in high-order harmonic generation from finite systems, Phys. Rev. A **105**, 053118 (2022).

[33] J. Masur, D. I. Bondar, and G. McCaul, Optical distinguishability of Mott insulators in the time versus frequency domain, Phys. Rev. A **106**, 013110 (2022).

[34] M. Udono, K. Sugimoto, T. Kaneko, and Y. Ohta, Excitonic effects on high-harmonic generation in Mott insulators, Phys. Rev. B **105**, L241108 (2022).

[35] Y. Murakami, K. Uchida, A. Koga, K. Tanaka, and P. Werner, Anomalous Temperature Dependence of High-Harmonic Generation in Mott Insulators, Phys. Rev. Lett. **129**, 157401 (2022).

[36] K. Uchida, G. Mattoni, S. Yonezawa, F. Nakamura, Y. Maeno, and K. Tanaka, High-order harmonic generation and its unconventional scaling law in the Mott-insulating Ca_2RuO_4, Phys. Rev. Lett. **128**, 127401 (2022).

[37] O. Grånäs, I. Vaskivskyi, X. Wang, P. Thunström, S. Ghimire, R. Knut, J. Söderström, L. Kjellsson, D. Turenne, R. Y. Engel, M. Beye, J. Lu, A. H. Reid, W. Schlotter, G. Coslovich, M. Hoffmann, G. Kolesov, C. Schüßler-Langeheine, A. Styervoyedov, N. Tancogne-Dejean, M. A. Sentef *et al.*, Ultrafast modification of the electronic structure of a correlated insulator, arXiv:2008.11115.

[38] M. R. Bionta, E. Haddad, A. Leblanc, V. Gruson, P. Lassonde, H. Ibrahim, J. Chaillou, N. Émond, M. R. Otto, A. Jiménez-Galán, R. E. F. Silva, M. Ivanov, B. J. Siwick, M. Chaker, and F. Légaré, Tracking ultrafast solid-state dynamics using high harmonic spectroscopy, Phys. Rev. Res. **3**, 023250 (2021).

[39] P. A. Lee, N. Nagaosa, and X.-G. Wen, Doping a Mott insulator: Physics of high-temperature superconductivity, Rev. Mod. Phys. **78**, 17 (2006).

[40] M. Imada, A. Fujimori, and Y. Tokura, Metal-insulator transitions, Rev. Mod. Phys. **70**, 1039 (1998).

[41] F. Gebhard, *The Mott Metal-Insulator Transition*, Vol. 137 (Springer, Berlin, 1997).

[42] S. Maekawa, *Physics of Transition Metal Oxides*, 1st ed., Springer Series in Solid-State Sciences, Volume 144 (Springer, Berlin, 2004).

[43] S. Mazumdar and A. N. Bloch, Systematic Trends in Short-Range Coulomb Effects among Nearly One-Dimensional Organic Conductors, Phys. Rev. Lett. **50**, 207 (1983).

[44] Z. Chen, Y. Wang, S. N. Rebec, T. Jia, M. Hashimoto, D. Lu, B. Moritz, R. G. Moore, T. P. Devereaux, and Z.-X. Shen, Anomalously strong near-neighbor attraction in doped 1 D cuprate chains, Science **373**, 1235 (2021).

[45] F. H. L. Essler, H. Frahm, F. Göhmann, A. Klümper, and V. E. Korepin, *The One-Dimensional Hubbard Model* (Cambridge University Press, Cambridge, 2005).

[46] N. Tomita and K. Nasu, Quantum fluctuation effects on light absorption spectra of the one-dimensional extended Hubbard model, Phys. Rev. B **63**, 085107 (2001).

[47] N. Klemke, O. D. Mücke, A. Rubio, F. X. Kärtner, and N. Tancogne-Dejean, Role of intraband dynamics in the generation of circularly polarized high harmonics from solids, Phys. Rev. B **102**, 104308 (2020).

[48] T. J. Park and J. C. Light, Unitary quantum time evolution by iterative Lanczos reduction, J. Chem. Phys. **85**, 5870 (1986).

[49] E. S. Smyth, J. S. Parker, and K. Taylor, Numerical integration of the time-dependent Schrödinger equation for laser-driven helium, Comput. Phys. Commun. **114**, 1 (1998).

[50] X. Guan, O. Zatsarinny, K. Bartschat, B. I. Schneider, J. Feist, and C. J. Noble, General approach to few-cycle intense laser interactions with complex atoms, Phys. Rev. A **76**, 053411 (2007).

[51] A. L. Frapiccini, A. Hamido, S. Schröter, D. Pyke, F. Mota-Furtado, P. F. O'Mahony, J. Madroñero, J. Eiglsperger, and B. Piraux, Explicit schemes for time propagating many-body wave functions, Phys. Rev. A **89**, 023418 (2014).

[52] M. B. Gaarde, J. L. Tate, and K. J. Schafer, Macroscopic aspects of attosecond pulse generation, J. Phys. B: At., Mol. Opt. Phys. **41**, 132001 (2008).

[53] G. D. Mahan, *Many-Particle Physics* (Kluwer Academic, New York, 2000), p. 24.

[54] N. A. Lima, L. N. Oliveira, and K. Capelle, Density-functional study of the Mott gap in the Hubbard model, Europhys. Lett. **60**, 601 (2002).

[55] M. S. Hybertsen, M. Schlüter, and N. E. Christensen, Calculation of Coulomb-interaction parameters for La_2CuO_4 using a constrained-density-functional approach, Phys. Rev. B **39**, 9028 (1989).

[56] H. Nishidome, K. Nagai, K. Uchida, Y. Ichinose, Y. Yomogida, Y. Miyata, K. Tanaka, and K. Yanagi, Control of high-harmonic generation by tuning the electronic structure and carrier injection, Nano Lett. **20**, 6215 (2020).

[57] C. Yu, K. K. Hansen, and L. B. Madsen, Enhanced high-order harmonic generation in donor-doped band-gap materials, Phys. Rev. A **99**, 013435 (2019).